



DISTRIBUTION STATEMENT A
Approved for public release
Distribution Unlimited

EXPERIMENTAL INVESTIGATION
OF THE INFLUENCE OF MOLECULAR WEIGHT
ON MIXING AND PENETRATION IN SUPERSONIC DISSIMILAR
GASEOUS INJECTION INTO A SUPERSONIC CROSS-FLOW

THESIS

Troy A. Giese, Captain, USAF

AFIT/GAE/ENY/97D-03

DTIC QUALITY INSPECTED-4

**DEPARTMENT OF THE AIR FORCE
AIR UNIVERSITY**

AIR FORCE INSTITUTE OF TECHNOLOGY

Wright-Patterson Air Force Base, Ohio

19980210 050

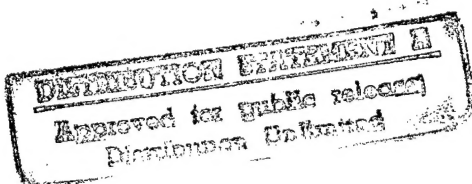
AFIT/GAE/ENY/97D-03

EXPERIMENTAL INVESTIGATION
OF THE INFLUENCE OF MOLECULAR WEIGHT
ON MIXING AND PENETRATION IN SUPERSONIC DISSIMILAR
GASEOUS INJECTION INTO A SUPERSONIC CROSS-FLOW

THESIS

Troy A. Giese, Captain, USAF

AFIT/GAE/ENY/97D-03



Disclaimer Statement

The views expressed in this thesis are those of the author and do not reflect the official policy or position of the Department of Defense or the U.S. Government.

EXPERIMENTAL INVESTIGATION
OF THE INFLUENCE OF MOLECULAR WEIGHT
ON MIXING AND PENETRATION IN SUPERSONIC DISSIMILAR
GASEOUS INJECTION INTO A SUPERSONIC CROSS-FLOW

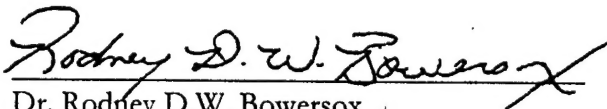
Troy A. Giese
Captain, USAF

Approved:



Dr. Jeffery K. Little, Major, USAF
Committee Chairman

3 Dec 97
Date



Dr. Rodney D.W. Bowersox
Committee Member

2 Dec '97
Date



Dr. Milton E. Franke
Committee Member

3 Dec 97
Date

AFIT/GAE/ENY/97D-03

EXPERIMENTAL INVESTIGATION
OF THE INFLUENCE OF MOLECULAR WEIGHT
ON MIXING AND PENETRATION IN SUPERSONIC DISSIMILAR
GASEOUS INJECTION INTO A SUPERSONIC CROSS-FLOW
THESIS

Presented to the Faculty of the School of Engineering of the

Air Force Institute of Technology

Air University

Air Education and Training Command

In Partial Fulfillment of the Requirements for the
Degree of Master of Science in Aeronautical Engineering

Troy A. Giese, B.S.A.E.

Captain, USAF

December 1997

Approved for public release; distribution unlimited

Acknowledgments

This work was made possible through the expert guidance of my thesis advisor, Dr. Rodney D.W. Bowersox. He provided me with just the right amount of help when needed while allowing me to work independently. Major Jeff Little, my co-advisor, did a yeoman's job in picking up my project midstream. The assistance of Dr. Raymond Fuller was invaluable. The gas analyzer equipment worked flawlessly. Special thanks goes to Mr. Andy Pitts, my lab technician, who kept the tunnel in working order. I would also like to thank the efforts of the reading committee, who had to suffer through the drafts. Finally, thanks goes to my family and friends for their patience and understanding.

Troy A. Giese

Table of Contents

	Page
Acknowledgments	ii
Table of Contents	iii
List of Figures.....	v
List of Tables	vi
List of Symbols.....	vii
Abstract	ix
1. Introduction.....	1.1
1.1 Motivation	1.1
1.2 Background	1.2
1.3 Scope of Present Study.....	1.3
1.4 Limitations of Present Study	1.3
2. Background.....	2.1
2.1 Flow Fundamentals.....	2.1
2.2 Transverse Injection.....	2.2
2.3 Vorticity Generation	2.3
2.4 Gas Sampling	2.4
3. Facilities and Instrumentation	3.1
3.1 AFIT Mach Three Wind Tunnel.....	3.1
3.2 Transverse Injector Model.....	3.2
3.2.1 Tunnel Coordinate System and Dimensions	3.4
3.3 PME Ramp.....	3.5
3.4 Measurement Locations	3.5
3.5 Mean Flow Measurements	3.5
3.5.1 Pressure Probes	3.5
3.5.2 Probe Traverse System.....	3.6
3.5.3 Data Acquisition.....	3.6
3.6 Gas Sampling	3.6
3.6.1 Sampling Probe	3.7
3.6.2 Gas Analyzer.....	3.7
3.6.3 Electronics	3.7
3.7 Flow Visualization.....	3.8
3.8 Other Computational Resources.....	3.8

4. Data Reduction	4.1
4.1 Mean Pressure Measurements	4.1
4.1.1 Pressure Ratio	4.1
4.2 Gas Concentration	4.2
4.3 Mach Number	4.3
5. Results and Analysis	5.1
5.1 Helium Injection	5.1
5.1.1 Flow Visualization	5.1
5.1.2 Concentration	5.3
5.1.3 Mach	5.3
5.1.4 Pressure	5.5
5.2 Argon Injection	5.5
5.2.1 Flow Visualization	5.5
5.2.2 Concentration	5.7
5.2.3 Mach	5.7
5.2.4 Pressure Data	5.9
5.3 Gas Comparison	5.9
6. Conclusions and Recommendation	6.1
6.1 Conclusions	6.1
6.2 Recommendation	6.1
Appendix A: Uncertainty Analysis	A.1
A. 1 Position Uncertainty	A.1
A. 2 Pressure Data Uncertainty	A.1
A. 3 Gas Analyzer Uncertainty	A.2
Vitae	V.1
Bibliography	B.1

List of Figures

Figure	Page
Figure 2.1: Example injection schlieren	2.2
Figure 2.2: Simple transverse injection	2.2
Figure 3.1: Side view of test section	3.2
Figure 3.2: Tunnel coordinate system	3.4
Figure 4.1: Argon calibration curves	4.2
Figure 5.1: Schlieren photograph of helium injection with no ramp	5.2
Figure 5.2: Schlieren photograph of helium injection with ramp	5.2
Figure 5.3: Helium concentration contour	5.3
Figure 5.4: Helium Mach contour	5.4
Figure 5.5: Helium total pressure ratio	5.4
Figure 5.6: Schlieren photograph of argon injection with no ramp	5.6
Figure 5.7: Schlieren photograph of argon injection with ramp	5.6
Figure 5.8: Argon concentration contour	5.7
Figure 5.9: Argon Mach contour	5.8
Figure 5.10: Argon total pressure ratio	5.8

List of Tables

Figure	Page
Table 3.1. Injector jet flow conditions.....	3.3
Table 3.2. Wind tunnel and injector nozzle exit dimensions	3.4
Table 3.3. Freestream flow conditions	3.4

List of Symbols

a, b	Empirically determined constants
A	Area, cm ²
Ar	Argon
C	Critical flow function
c_p	Specific heat at constant pressure, J/kg·K
d	Injector nozzle exit diameter, mm
He	Helium
I	Current, A
k	Thermal conductivity, W/m·K
l	Length of hot-film, mm
M	Mach number
Nu	Nusselt number
q	heat transfer rate, W
\bar{q}	Dynamic pressure ratio, $(\rho u^2)_i / (\rho u^2)_\infty$
P	Pressure, Pa
R	Specific gas constant, J/kg·K or Resistance, Ω
\mathcal{R}	Universal gas constant, J/kmol·K
Re	Reynolds number
\mathcal{T}	Molecular weight, kg/kmol
U, u	Velocity, m/s
V	Voltage, V _{dc}
X	Mole fraction
x	Streamwise tunnel coordinate
y	Vertical tunnel coordinate
z	Horizontal tunnel coordinate

Greek

γ	Ratio of specific heats
ρ	Density, kg/m ³
λ	Mass flux ratio, $(\rho u)_i/(\rho u)_\infty$
μ	viscosity, kg/s·m

Subscripts

0	Upstream property
1	Local property
2	Pitot probe property
air	Air property
c	Sensor plane or Cone-static
f	Hot-film property
gas	Gas property
i	Injector property
m	Injector nozzle major axis
s	Series bridge property
t	Total property

Superscript

$*$	Choked condition
$+$	Upper bound
$-$	Lower bound

Abstract

In pursuit of a more efficient and effective fuel-air mixing for a SCRAMjet combustor, this study investigated relative near field effects of molecular weight on mixing and penetration of different gaseous injection into a supersonic ($M=2.9$) cross flow. Helium and argon gas were chosen as injectants because of the large differences in molecular weights. Also, mixing enhancement was observed by injecting the traverse gas jet parallel to the compression face of a ramp. Color schlieren photography was used to identify the shock structures and interactions in the flow field. Measurements of mean flow properties were used to establish the jet plume size, penetration, and concentration and to quantify the total pressure loss. Results indicate greater mixing and plume expansion can be achieved with helium compared to argon.

EXPERIMENTAL INVESTIGATION OF THE INFLUENCE OF MOLECULAR WEIGHT ON MIXING AND PENETRATION IN SUPERSONIC DISSIMILAR GASEOUS INJECTION INTO A SUPERSONIC CROSS-FLOW

1. Introduction

1.1 Motivation

The early decades of aviation were characterized by the pursuit of speed and altitude. A major push for higher speed was initiated by the X-series of aircraft that explored the supersonic flight regime in the 1950s and 1960s.¹ Since that time, air-breathing propulsion systems have pushed material and chemical properties to the limits. Because of these limits, progress in the field has been evolutionary rather than revolutionary since the early 1960s.² Material sciences and computational resources have allowed systems to become more efficient, but the great strides in the "higher and faster" progression seen in the late 1950s have stopped. The SR-71, a late 1950s design, still holds the speed records for air-breathing manned aircraft at Mach 3+. The unmanned D-21 was ramjet powered and achieved Mach 5+. The experimental X-15, while achieving nearly Mach 7, was rocket powered.³ The benefits of a hypersonic air-breathing aircraft are obvious. By utilizing the oxygen in the atmosphere, the aircraft only needs to carry the fuel, therefore increasing the payload or range. The speed of such aircraft is also desired by planners for fast worldwide coverage and as a platform for orbit insertion. These benefits have been shaped in recent years into requirements for the National Aerospace Plane and currently the "Military Spaceplane."⁴

For speeds in excess of Mach 4, a transition from turbofan or turbojet to the ramjet mode of propulsion is necessary. The characteristics of the conventional subsonic combusting ramjet are well understood. However, the performance of the subsonic

combusting ramjet deteriorates at hypersonic speeds due to real gas effects and internal losses, and the structural integrity of the engine becomes very difficult or impossible to maintain due to the high internal temperatures and pressures. Thus, it is necessary to utilize the supersonic combustion engine (SCRAMjet) for such high speeds.

The SCRAMjet engine potentially offers outstanding specific impulse performance at hypersonic Mach numbers. The loss of energy in the flow through the engine is less than in a ramjet engine, but supersonic combustion represents a major technological challenge in engine development. The existence of supersonic throughflow presents the problem of how to manage efficient and effective mixing and burning of fuel for the extremely short residence time the working fluid is in the combustion chamber.

1.2 Background

The short residence time of flow inside the combustor engine presents a problem to designers which must be overcome by enhancing the mixing and penetration of the fuel in the oxidizer. To aid in the mixing and penetration of an injected plume into a supersonic freestream, several schemes have been studied. Early studies focused on the effects of underexpanded jets injected normally into the flow.^{5,6} While laying the foundation of today's computational approaches, these initial efforts provided fundamental analyses of the governing equations. The pressure differential across the front to rear face of the emerging jet was found to enhance mixing.^{7,8} In addition to transverse injection,^{9,10,11} more recent studies have focused on retaining the jet momentum in the direction of thrust through low angle injection over or behind ramps.^{2,12,13,14,15} These configurations were designed to generate vorticity from the spillage of high pressure air off and around the leading compression surface.¹⁷

Along with the study of mixing enhancements, a parallel effort has been made to quantify the concentrations of binary gas mixtures. Many of these studies have focused on using a hot-wire probe to make calibration curves for known concentrations and pressures.^{16,17,18}

1.3 Scope of Present Study

The primary objective of this study is to compare the differences molecular weight has on the mixing and penetration of an injectant gas into a supersonic crossflow. This is accomplished by examination of the near field mixing of Mach 1.87 underexpanded supersonic helium and argon jets transversely injected 25° into a nominally Mach 2.9 air freestream. Also, a comparison is made between a simple transverse injection and injection over a penetration and mixing enhancement ramp.

Helium and argon were chosen for the large differences in molecular weights between the two. Helium has a molecular weight of approximately 4 while argon has a molecular weight of approximately 40. Also, these weights approximate the trends found in the two most likely fuels, hydrogen and hydrocarbons, for SCRAMjet applications. An extremely light fuel and a fuel with a weight an order of magnitude greater.

1.4 Limitations of Present Study

Limitations of this study include availability of facilities and equipment, number of downstream locations sampled, and available data. A time constraint imposed on the use of shared resources limited the mean flow and concentration measurements to one axial station downstream of the injection site. The limitation in downstream test location is partially overcome by the fact the fuel plume under proposed flight conditions of a hypersonic

vehicle will most likely combust in the near-field due to the extreme high temperatures to be expected in the flow.¹⁹ These limitations on the data collected affect the understanding of the detail mechanisms acting in the flow and more analyses of the near-field is needed before a complete understanding is attained.

2. Background

There have been many experimental and computational studies in the field of transverse supersonic injection and gas sampling. This chapter reviews some of this research from past investigations. The topics covered are flow and injection fundamentals, transverse injection, vorticity generation, and gas sampling.

2.1 Flow Fundamentals

Several flow variables and injection parameters have been established to aide in the comparison of flows at different conditions. The injection parameters include injector-to-freestream ratios such as the velocity ratio, mass flux ratio, and expansion ratio.⁹ The dynamic pressure ratio, \bar{q} , is another injector-to-freestream ratio that is also known as the momentum flux ratio. The primary variables of concern for this study are the injector diameter based Reynolds number, d , the boundary layer depth to injector diameter ratio, $\frac{\delta}{d}$, and the flow total properties.

Injection of an underexpanded sonic or supersonic jet into a supersonic crossflow produces several flow structures. Figure 2.1 shows some of these features described below. First, a bow shock is produced as the freestream impacts the injection streamtube as if the injectant were a cylindrical body.⁷ A separation bubble can form slightly upstream of the injector port when $\frac{\delta}{d}$ is on the order of one or more. This is due to the boundary layer being thicker than the injector diameter. After entering the freestream, the jet experiences a rapid Prandtl-Meyer expansion surrounded by a barrel shock.¹¹ A shock that is normal to the jet path terminates the barrel shock and recompresses the flow. This shock is known as the Mach disk and large scale mixing occurs after this normal shock.

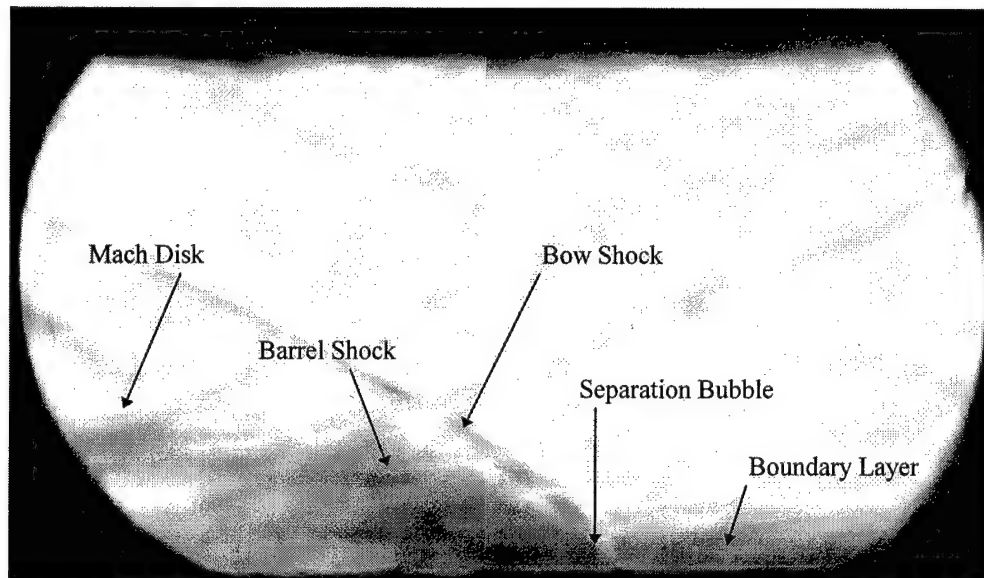


Figure 2.1: Example injection schlieren

2.2 Transverse Injection

Transverse injection is the simplest injection configuration. It requires only an injection port at the desired injection angle, usually normal to the plane of the injection wall and parallel with the direction of flow. Figure 2.2 illustrates the simple transverse injection used in this study.

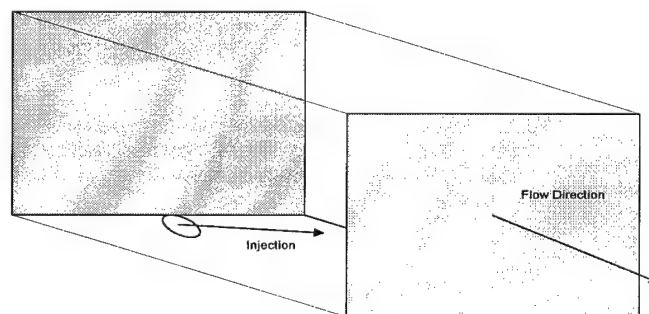


Figure 2.2: Simple transverse injection

The entry of the injectant is treated as a two stage process.⁶ The jet remains relatively intact as it first enters the freestream and then expands to the height of the Mach disk. Beyond the Mach disk, the flow turns and accelerates with the main flow. In the second stage the jet acts as a coaxial vortex mixing structure.

The dynamic pressure ratio, \bar{q} , strongly impacts mixing and penetration in the near-field. The initial rate of mixing is proportional to $\frac{1}{\bar{q}}$.⁹ This can be interpreted from continuity and momentum principles. As the dynamic pressure of the injectant is increased, the injectant will initially enter the freestream either faster or denser. If the injectant were faster, the jet itself would reduce the residence time it has to mix in the local freestream. If it were denser, it would require greater time and distance to disperse. Penetration is enhanced with increasing \bar{q} in that the Mach disk is pushed further out into the freestream.⁶

2.3 Vorticity Generation

Vorticity is the driving mixing mechanism in the near field.⁷ Streamwise vorticity is generated by two mechanisms in transverse injection. The first is the external pressure differential created across the front and rear faces of the emerging jet. The main flow must split around the injectant jet, creating high pressure regions on the front and sides of the jet. The resulting low pressure on the rear of the jet becomes an entrainment region for the local freestream. This results in a counter-rotating vortex pair inside the injectant jet. The second mechanism is created as the plume is bent coaxially with the freestream. The inside region of the plume which is not as greatly accelerated is drawn into the center of the plume.

For injection over a ramp, the primary vortex generation comes from the ramp, not the injectant plume. Flow pressurization occurs in the shock layer between the ramp induced

bow shock and the ramp compression face. The high pressure fluid then spills around the ramp causing a streamwise vorticity.¹² The vorticity causes large scale convective mixing that forms a counter-rotating vortex pair.⁸ The relative strength of the vorticity generated depends on the freestream Mach number. Additional vorticity is imparted by the pressurized flow expanding over the rear face of the ramp and wrapping around the low pressure region encircling the underexpanded jet plume.¹³

Once the counter-rotating vortex pair is generated, it is the dominant mixing mechanism in the near field.^{7,8} A cross section view of the developed plume remains circular with the vortex structures clearly visible with intense rotation rates.²⁰

2.4 Gas Sampling

For the complete description of a flowfield generated by a fully-constrained supersonic flow with foreign gas injection, it is necessary to obtain species composition measurements. Gas injection creates a mixture of different species with different ratios of specific heats, γ . Nearly all of the equations relating thermodynamic variables to Mach number involve γ as an exponential power. Therefore, only a slight variation may cause significant changes in reduced thermodynamic values.

The major addition to this study over previous studies was the different gas injectants used. Because of this, the method of finding the concentration levels and therefore γ will be discussed in detail here. The concentration measurement probe was designed to include a hot-film sensor, pressure tap, and thermocouple. The condition for mass continuity is expressed as

$$\rho u = P_t \sqrt{\frac{\gamma}{RT_t}} M \left[1 + \frac{\gamma-1}{2} M^2 \right]^{\frac{-(\gamma+1)}{2(\gamma-1)}} \quad (2.1)$$

Since the flow through the analyzer is choked ($M=1$)²³, this continuity equation reduces to

$$(\rho u)^* = \frac{P_t C^*}{\sqrt{T_t}} \quad (2.2)$$

where C^* is the critical flow function defined by

$$C^* = \sqrt{\frac{\gamma \mathfrak{F}}{\mathfrak{R}}} \left[\frac{2}{\gamma+1} \right]^{\frac{(\gamma+1)}{2(\gamma-1)}} \quad (2.3)$$

where the * designates sonic conditions at the orifice and \mathfrak{F} is the molecular weight. Since the mass flow through the sensor plane must equal the mass flow through the choked orifice, the mass flux at the sensor plane may be expressed as

$$\rho u = \frac{P_t C^*}{\sqrt{T_t}} \frac{A^*}{A_c} \quad (2.4)$$

Hence, the mass flux through the sensor plane is a function of the total pressure, total temperature, area ratio, and gas composition.

Now consider the heat transfer from the hot-film sensor at the measurement plane to the passing fluid. The rate of heat transfer is given by

$$q_f = I_f^2 R_f \quad (2.5)$$

where R_f is the film resistance and I_f is the film current supplied by the anemometer.²³ For a constant temperature anemometer, the film current is related to the anemometer response voltage by

$$I_f = \frac{V}{R_f + R_s} \quad (2.6)$$

where R_s is the series bridge resistance. Now define the Nusselt number in terms of the rate of heat transfer from the hot-film and the temperature difference between the film and the passing fluid as

$$Nu \equiv \frac{q_f}{\pi k l (T_f - T_i)} \quad (2.7)$$

where k is the thermal conductivity of the gas mixture and l is the active sensing length of the hot-film.²³ Then, combining Equations 2.4, 2.5, and 2.6, the Nusselt number may be expressed as

$$Nu = \frac{R_f}{(R_f + R_s)^2} \frac{V^2}{\pi k l (T_f - T_i)} \quad (2.8)$$

The Nusselt number may also be related to the mass flux via the Reynolds number,

$Re = \frac{\rho u d}{\mu}$, where d is the film diameter, as

$$Nu = a \left(\rho u \frac{d}{\mu} \right)^b \quad (2.9)$$

and a and b are empirically determined constants. Thus equating equations 2.7, 2.8, and 2.9 for Nusselt number and inserting Equation 2.4 for mass flux at the sensor plane, the governing equation for the anemometer response voltage is obtained as

$$V^2 = \frac{(R_s + R_f)^2}{R_f} \pi l k a \left(\frac{d}{\mu} \frac{P_t}{\sqrt{T_f}} \frac{A^*}{A_c} C^* \right)^b (T_f - T_t) \quad (2.10)$$

The parameters a , b , C^* , k , and μ are properties of the gas mixture and are therefore a function of the gas concentration, X_{gas} . Furthermore, since a constant temperature anemometer is employed, the film resistance T_f and therefore R_f are constant. Finally, the values of l , d , and R_s are system parameters and remain constant. Therefore the anemometer response voltage is a function of the total pressure, P_t , the total temperature T_t , and the gas concentration, X_{gas} . That is

$$V = f(P_t, T_t, X_{gas}) \quad (2.11)$$

Thus for a given total pressure and total temperature, the gas concentration is uniquely determined by the anemometer response voltage. It is this voltage that is recorded for each concentration and pressure during the calibration and data runs. Fuller presents a detailed derivation of the concepts presented in this section.²³

3. Facilities and Instrumentation

This chapter contains descriptions of the facilities and instrumentation used during this investigation. Descriptions of the AFIT Mach three wind tunnel, the transverse injector, PME ramp, mean flow probes and gas-sampling instrumentation are presented followed by descriptions of the data acquisition system.

3.1 AFIT Mach Three Wind Tunnel

The tests for this investigation were conducted using the AFIT Mach three wind tunnel. This tunnel was a blow-down design, using a pressure-vacuum system. The building-supplied pressurized air was provided by two Atlas Copco GAU 807 compressors at a 0.5 kg/s flow rate. The air was dried by two Pioneer R500A refrigerant air dryers en route to the pressure side of the tunnel. Final drying and filtering was performed by a cyclone separator and multiple layers of Filtrite® filter paper.

Sixteen vacuum tanks of 16 m³ volume each comprised the vacuum system. The evacuation was accomplished by three Stokes Micro Vac pumps and the tanks were evacuated to approximately 10.0 mm Hg prior to each run. This provided over twice as much run time as was needed during this investigation.

The tunnel itself consisted of a plenum chamber upstream of a converging-diverging nozzle to produce supersonic flow. Flow straightening screens were placed between the air supply and plenum chamber. An Endevco 0-960 kPa pressure transducer mounted in the plenum chamber measured total gauge pressure. Fluctuation in total pressure during test runs were no more than $\pm 1.5\%$. An Omega Engineering type K thermocouple provided plenum total temperature. Fluctuations in total temperature during test runs were no more

than $\pm 0.5\%$. The nominal Mach number of the tunnel nozzle is 2.8, $\pm 1.8\%$ with a standard operating total temperature of 294K²¹

3.2 Transverse Injector Model

The injector model is described in full detail by McCann.²⁰ The injector setup was originally used to research turbulence at low angles of injection. Wilson made minor modifications to the injector model, incorporating PME ramps to study the enhancements of mixing associated with the ramps and to provide smoother flow from the injector.²² Since the primary objective of this study is to measure differences in penetration and mixing of different injectant gasses, no further modifications were made to the transverse injector. Figure 3.1 is a side view of the test section.

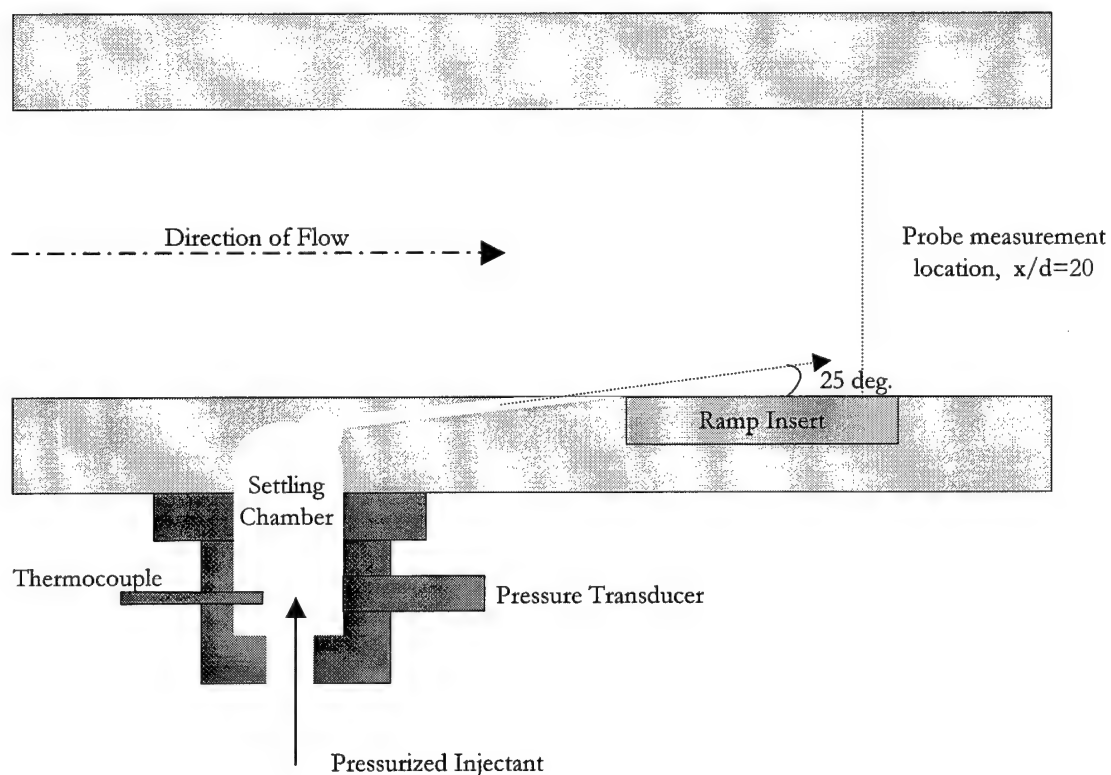


Figure 3.1: Side view of test section

The throat diameter of the injector outlet was 0.32 cm expanding to 0.40 cm across the exit minor axis. The settling chamber was monitored by an Endevco 0-690 kPa pressure transducer. A high pressure line was attached through a regulator from the gas bottles to supply argon and helium. The gas first traveled through 2 meters of copper tubing to ensure the injectant gas was at the same total temperature as the freestream. An Omega Engineering type K thermocouple was inserted in the settling chamber of the injector to monitor this temperature. Table 3.1 summarizes the injector jet conditions. The variations in the following parameters were no more than 2.3%.

Table 3.1. Injector jet flow conditions

Mach	1.82
P_{oi}	304541 Pa
T_{oi}	294 K
P_i	47595 Pa
T_i	173 K
U_i (He)	1409.8 m/s
U_i (Ar)	445.9 m/s
γ (He)	1.67
γ (Ar)	1.67
λ (He)	1.24
λ (Ar)	3.93
\bar{q} (He)	2.89
\bar{q} (Ar)	2.89

It is interesting to note that \bar{q} is the same for both helium and argon. This is due to the differences in density and velocity for each of these gases. While helium has a low density, the velocity is high, which makes the dynamic pressure ratio with constant injector pressure equal to argon with a high density but low velocity.

3.2.1 Tunnel Coordinate System and Dimensions

The tunnel coordinate system relative to the injector nozzle exit is summarized in Figure

3.2.

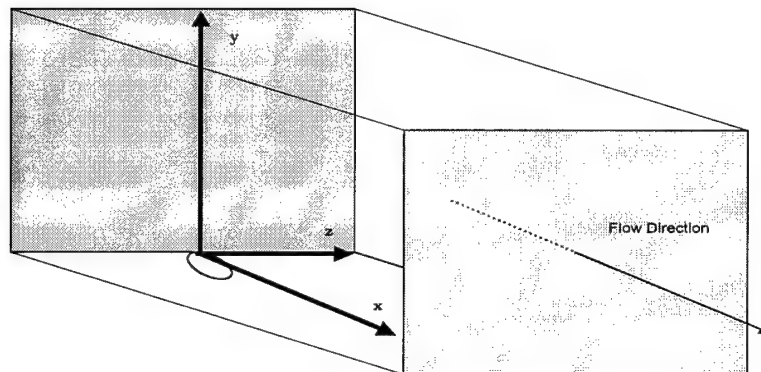


Figure 3.2: Tunnel coordinate system

The physical dimensions of the tunnel and injector are summarized in Table 3.2 below.

Table 3.2. Wind tunnel and injector nozzle exit dimensions

Test Section Width	6.35 cm
Test Section Height	6.35 cm
Test Section Length	35.0 cm
Nozzle Exit Minor Axis Diameter, d	0.40 cm
Nozzle Exit Major Exit Diameter, d_m	0.92 cm
Distance from Tunnel Nozzle to Test Section	27.0 cm
Position of Injector Exit on Test Section	8.5 cm (from test section leading edge)

The standard freestream conditions for a nominal test run are given in Table 3.2.

Table 3.3. Freestream flow conditions

Mach	2.9
P_o	217875 Pa
T_o	294 K
P	8028 Pa
T	114 K
U_o	608 m/s

3.3 PME Ramp

Along with a flat plate, a single penetration and mixing enhancement ramp, the symmetric ramp, SR 3, used by Wilson, was chosen for the study.²² This ramp was symmetric about the y - z plane of the tunnel coordinate system. This ramp introduced a two-dimensional shock because of the flat plate compression surface. The plume interacts with this shock while the trailing edge accelerates the flow behind the ramp. See Wilson for complete design criteria and dimensions of this ramp.

3.4 Measurement Locations

The measurement location for the mean flow data was at $x/d=20$. Because of symmetry, the z direction horizontal coverage of the tunnel consisted of 10 stations spanning half of the width. Each station was 0.138 cm apart for an effective coverage of 4.0 cm. In the tunnel coordinate system, this was a range from -4.05 to +4.05 z/d . This allowed the same spatial resolution as Wilson for mean flow measurements.²² Vertically, the span covered was 2.54 cm or a y/d from 0.3 to 6.3.

3.5 Mean Flow Measurements

Mean flow measurements were acquired through a system consisting of pressure probes, transducers and a traverse mount described in the following sections.

3.5.1 Pressure Probes

A Pitot and cone-static probe were used to collect the mean flow data. The Pitot probe was constructed of 1.6 mm outer diameter stainless steel. The pressure was fed by Tygon tubing to an Endevco 0-103 kPa transducer. The cone-static probe consisted of four evenly spaced 0.34 mm ports that fed into a common chamber. This design has been shown to

allow a misalignment error of up to 6° off centerline of the flow without an effect on the measured pressure.²² The cone-static probe pressure was also fed through Tygon tubing into an Endevco 0-103 kPa transducer. The output of the transducer for both probes was filtered by an Endevco model 4225 signal conditioner. The signal conditioner was assigned and calibrated for each transducer used.

3.5.2 Probe Traverse System

The pitot and cone-static probes were swept through the vertically oriented y/d range for each of the 10 z axis stations across the tunnel cross section. The traverse system used was a Dantec 3-axis traverse system. The position of the traverse was recorded as a voltage by a TransTek Model 0217 linear voltage displacement transducer. The voltage-position relation was linear for the range of motion of the probes.

3.5.3 Data Acquisition

Data acquisition for the flow measurements was accomplished through a Dantec 90N10 based data acquisition board connected to an Acer Pentium computer. Dantec Streamware® software acquired the raw voltage readings collected by the pressure probes. The sample rate used for data acquisition on all channels was 400 Hz. The data were converted to tab delimited text files for processing by the data reduction routines.

3.6 Gas Sampling

Gas sampling for concentration measurements were obtained using an intrusive sampling probe and gas analyzer designed for supersonic flow by Fuller.²³

3.6.1 Sampling Probe

The probe used in the current study was first proposed by Ninnemann.²⁴ It consisted of a small Pitot tube with conical tip and an internal divergence. This ensured an isokinetic sample by swallowing the shock into the probe. The probe was constructed from stainless steel with an outer diameter of 3.18 mm. The sampling probe was approximately 25 cm long and was terminated by the gas analyzer. The probe was attached to the same traverse system described previously and measurements were taken over the same grid.

3.6.2 Gas Analyzer

The gas analyzer consisted of a rectangular (84mm x 36 mm x 19 mm) stainless steel block housing with a 3.86 mm bore through the center. The sensor plane consisted of a TSI 1220-20 high temperature platinum hot-film sensor mounted perpendicular to the flow entering the analyzer, a Genisco PB-923 pressure transducer with a range of 0 to 100 psia, and an Omega Engineering Type-K thermocouple. The flow then exited the probe through a choked orifice.

3.6.3 Electronics

Data acquisition was performed with a National Instruments AT-MIO-16X multifunction input/output board installed in a 486 rack-mounted computer. The AT-MIO-16D has a 10 μ sec, 16-bit, sampling ADC that can monitor up to 8 different channels with programmable gains.

The hot-film sensor was used in conjunction with a Dantec Type55M01 constant temperature anemometer fitted with a DISA Type-55M10 CTA standard bridge. The output from the sensor via the anemometer was passed through a Frequency Devices Model 9002

dual-channel programmable filter. The filtered signal was input into the computer via the AT-MIO-16X I/O board.

The pressure excitation voltage and output gain was supplied by a Measurements Group 23120 signal conditioning amplifier. The voltage-to-pressure calibration was obtained via a Druck DPI 500 pressure indicator. The output voltages for pressures ranging from 0 to 100 psia and temperatures ranging from 482 R to 1100 R were recorded using the above mentioned data acquisition system.

3.7 Flow Visualization

Color schlieren photographs were taken for each gas and ramp configuration. Due to the limited coverage provided by the optical glass side walls of the wind tunnel, two views were needed to form a composite image of the flowfield around the injector and ramp. The light source used was a Cordin Model 5401 arc light and aligned by hand. The light was collimated by a 153 cm focal length mirror and passed through the test section. A Nikon N90s camera with a Kodak DCS420 digital attachment was used to capture the images. The lens was a Tokina 80-200 mm telephoto with a Vivatar 2x macro focusing teleconverter.

3.8 Other Computational Resources

Data reduction was performed on an Ameritest Pentium PC. Contour plots were generated on the AFIT Sun Sparc 2 and 10 workstations using Tecplot 7.0. The schlieren images were generated by Adobe Photoshop.

4. Data Reduction

This chapter details the data reduction routines applied to the raw pressure probe data collected with the cone-static probe, the pitot probe, and the concentration probe.

4.1 Mean Pressure Measurements

For both flow pressure probes, the raw data were converted from gauge pressures to absolute pressures and reduced to mean pressure measurements. This was accomplished using a combination of VISUAL BASIC data reduction routines and EXCEL spreadsheets. The routines first scaled the probe voltages to psi by the appropriate factor depending on probe type. Second, the gauge psi values were converted to inches of mercury and added to the atmospheric pressure in the wind tunnel lab at the time of the data run. Third, the converted pressures were averaged by groups of 44 points into a single point. The spreadsheet also determined the position of the probes by averaging the same range of traverse position travel voltages into a single point. At the 400 Hz sample rate, 44 samples comprised 0.11 seconds of traverse movement. This span of movement covers 0.03 cm for each mean datum and provides a spatial resolution of 80 mean datum over the 2.54 cm of traversal.

4.1.1 Pressure Ratio

The ratio of the cone-static and pitot pressure data (P/P_{t2}) was determined. Because of the time required for each probe, gas, and ramp configuration, the cone-static and pitot pressure data were collected on separate wind tunnel runs, and on separate days in some instances. To eliminate the error caused by measuring the pressures on different runs, the

probe pressure ratios were normalized to each other with the recorded total pressure of the flow for the data run as shown in equation 4.1.

$$\frac{P_c}{P_{t2}} = \frac{P_c}{P_{t0}} \bigg/ \frac{P_{t2}}{P_{t0}} \quad (4.1)$$

4.2 Gas Concentration

First, a calibration of the gas concentration was performed. This consisted of two steps. A static air-gas mixture of known concentration, temperature and pressure was analyzed at different concentration level and pressure levels. Then the data was reduced using a VISUAL BASIC code to find the constants a and b from Equation 2.10. The calibration procedure for the gas analyzer also yielded a curve fit for the various given gas concentrations and a fixed calibration temperature. Figure 4.1 is the calibration curve for argon.

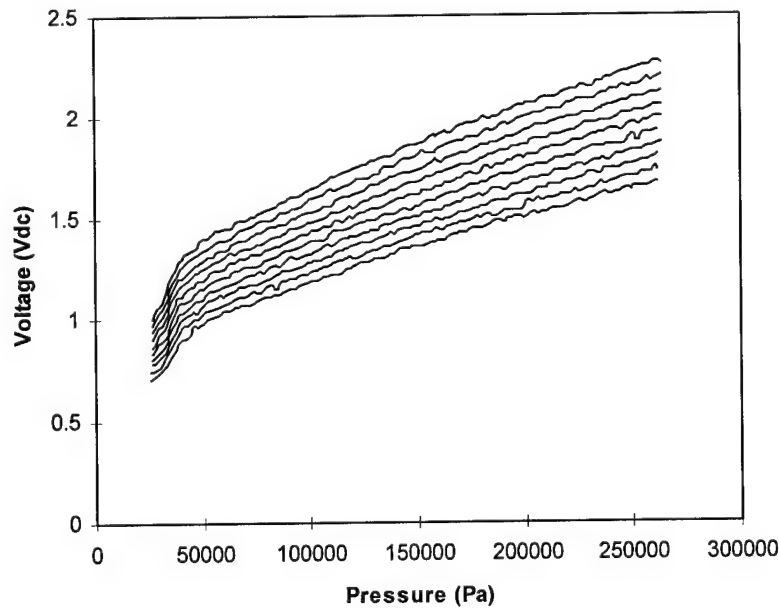


Figure 4.1: Argon calibration curves

These curve fits gave the hot-film voltage as a function of sampling pressure. Thus, for a pair of values, hot-film voltage and sampling pressure, the gas concentration could be interpolated provided the sampling temperature was close to the calibration temperature. For example, say that at a given sampling pressure and temperature, an anemometer response voltage of V is measured. On the calibration map, at the measured sampling pressure, this voltage is bounded by a higher voltage, V^+ , representing a higher gas mole fraction of X^+ and a lower voltage, V^- , representing a lower gas mole fraction of X^- . So that the linear interpolation²³ will yield the measured gas mole fraction as

$$X = \frac{X^+ - X^-}{V^+ - V^-} (V - V^-) + X^- \quad (4.2)$$

4.3 Mach Number

To determine the local Mach number, the pressure ratio and gas mole fraction were used as follows. First, the specific gas constant, R , for the local gas concentration was found by

$$R = \frac{\Re}{X\mathfrak{I}_{gas} + (1 - X)\mathfrak{I}_{air}} \quad (4.3)$$

Next a ratio of specific heats was determined by

$$c_p = \frac{\mathfrak{I}_{gas} X c_{p,gas} + \mathfrak{I}_{air} (1 - X) c_{p,air}}{\mathfrak{I}_{gas} M + (1 - X) \mathfrak{I}_{air}} \quad (4.4)$$

$$\gamma = \frac{c_p}{(c_p - R)} \quad (4.5)$$

Finally, the Mach number was determined from the ratio of cone-static to Pitot pressure,

P_c/P_{t2} and γ using a table look up. For supersonic flow over a cone, the governing equation was derived by Taylor.²⁵ This equation is a second order, non-linear, ordinary differential equation which requires a numerical solution. Taylor showed that the ratio of cone-static surface pressure, P_c , to the freestream pressure, P_t , is a function of the freestream Mach number, M_t , and γ . This ratio divided by the Rayleigh-Pitot formula yields the Mach number as a function of the ratio of cone-static to Pitot pressure, P_c/P_{t2} and γ . Thus, for a given cone-static pressure, Pitot pressure, and γ , the corresponding Mach number may be bilinearly interpolated using an appropriate look-up table. The Taylor-McColl equation was solved for a large range of Mach numbers. These solutions were combined with solutions of the Rayleigh-Pitot formula to form the table.

5. Results and Analysis

This chapter describes the flow field for each of the four configurations (two gases and two ramp configurations). For all configurations studied, the following order of analysis is used. First, schlieren flow visualization images are used for qualitative results. The basic flow shock structures along the centerline x - y plane are examined. Second, the gas mole fraction concentration, Mach number contour plots, and total pressure ratio contour plots are presented. The contour plots are presented as two half plots. Since the flow is symmetric about the x axis, only half of the flow is needed for each case. This allows easy comparison between two cases. Finally, the apparent effects of molecular weight are discussed.

5.1 Helium Injection

5.1.1 Flow Visualization

Figure 5.1 is the schlieren photograph of helium injection with no ramp. Figure 5.2 shows the case of helium injection with a ramp present. All of the shock structures discussed in section 2.1 can be seen in both photographs. Note the shock created parallel to the ramp face in figure 5.2. Also, the expansion of the flow behind the ramp is apparent.

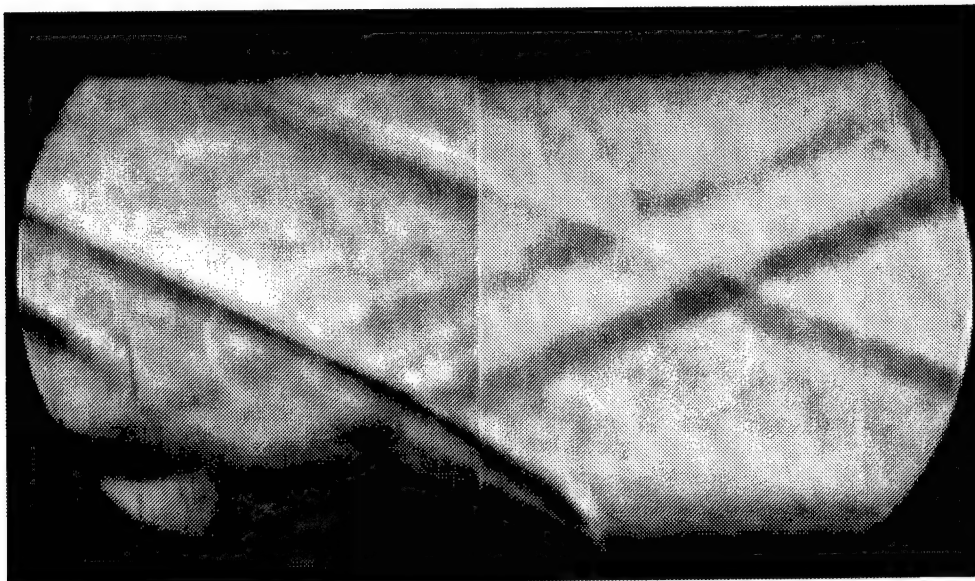


Figure: 5.1: Schlieren photograph of helium injection with no ramp

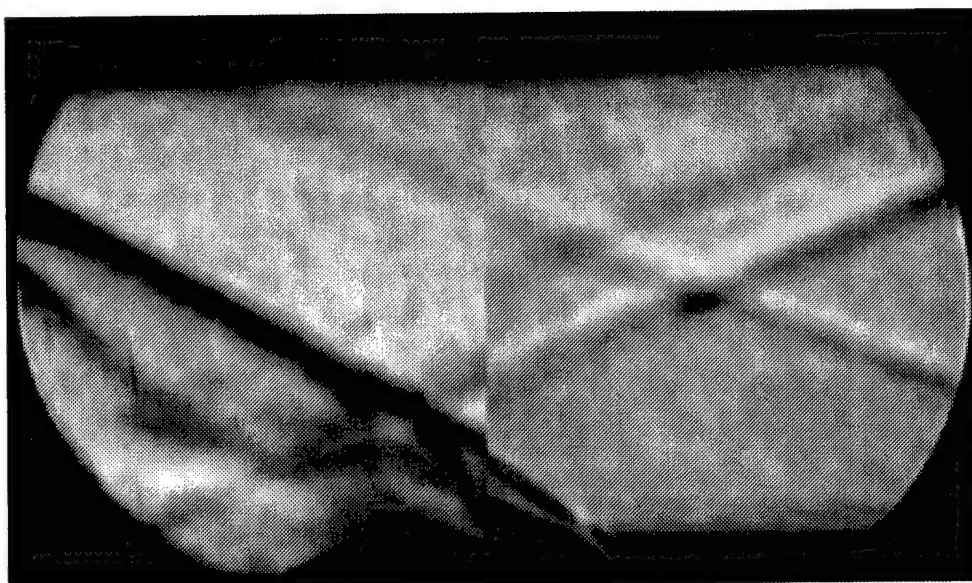


Figure: 5.2: Schlieren photograph of helium injection with ramp

5.1.2 Concentration

Figure 5.3 presents the molar concentration data for helium. The with-ramp configuration has a smaller area of concentrated helium at a core of the vortex while the no-ramp case has a large area of high concentration. The ramp helps to disperse the helium to a wider area of the plume, while the no-ramp case concentrates the helium within the plume. Also the plume area was computed as 17% larger with the ramp than without. This compares well with a 30% increase in plume size for injection with air.²²

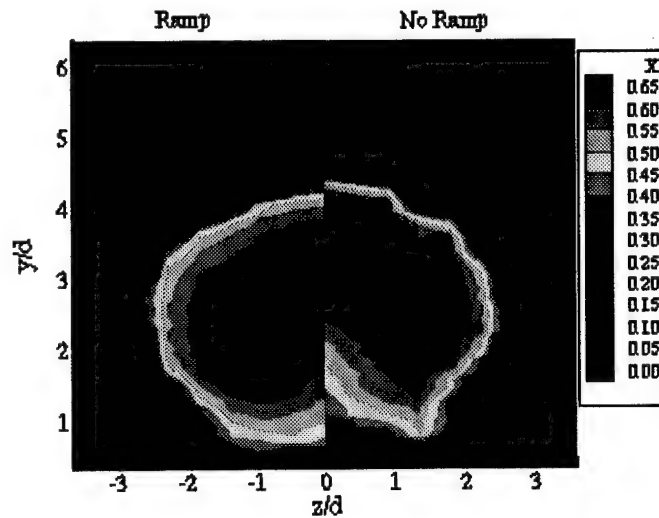


Figure 5.3: Helium concentration contour

5.1.3 Mach

As expected, the Mach contour shown in Figure 5.4 shows a low Mach number within the core of the plume for the ramp case, while without the ramp the plume has higher and more uniform Mach numbers. The plume size was found to be 23% larger with the ramp, giving consistent results with the plume area measured with concentration. This is also 300% the area of the plume found with air injection.²²

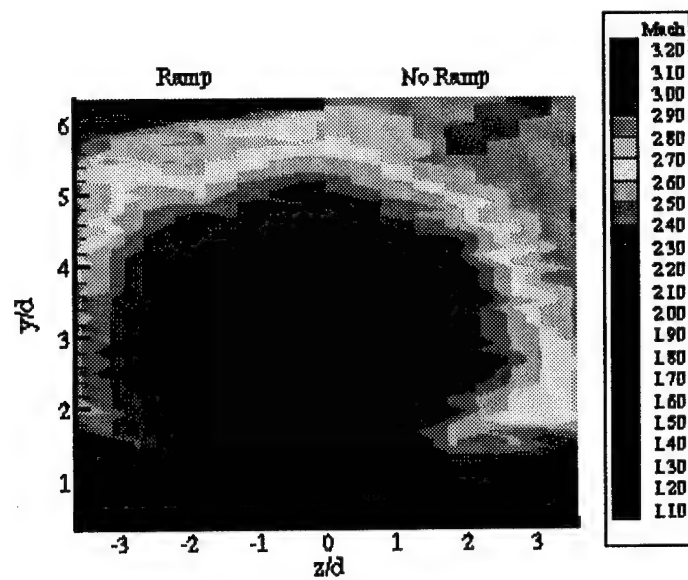


Figure 5.4: Helium Mach contour

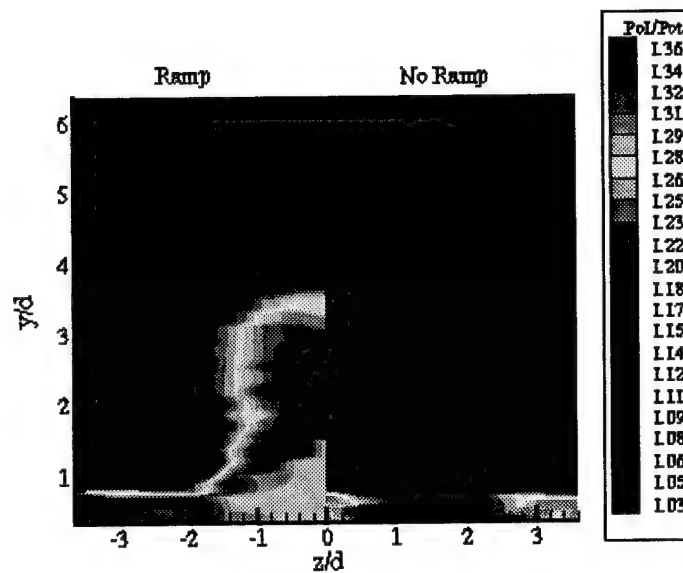


Figure 5.5: Helium total pressure ratio

5.1.4 Pressure

Figure 5.5 shows a comparison of the total pressure ratio with helium injection with and without the PME ramp. The ramp clearly increases the ratio within the plume. While the pressure loss from the ramp is not desirable, the additional mixing that is attained because of the ramp as seen in the Mach and concentration contours, outweighs this drawback. This data is consistent with prior study results.²² Compared to the simple traverse injection, the ramp results indicate the vorticity of the plume has been substantially diminished, but mixing and penetration is enhanced.

5.2 Argon Injection

5.2.1 Flow Visualization

Figure 5.6 is the schlieren photograph of argon injection with no ramp. Figure 5.7 shows the case of argon injection with a ramp present. Again, all of the shock structures discussed in section 2.1 can be seen in both photographs. Note the shock created parallel to the ramp face and expansion behind the ramp seen in figure 5.2 for helium are also present in figure 5.7.

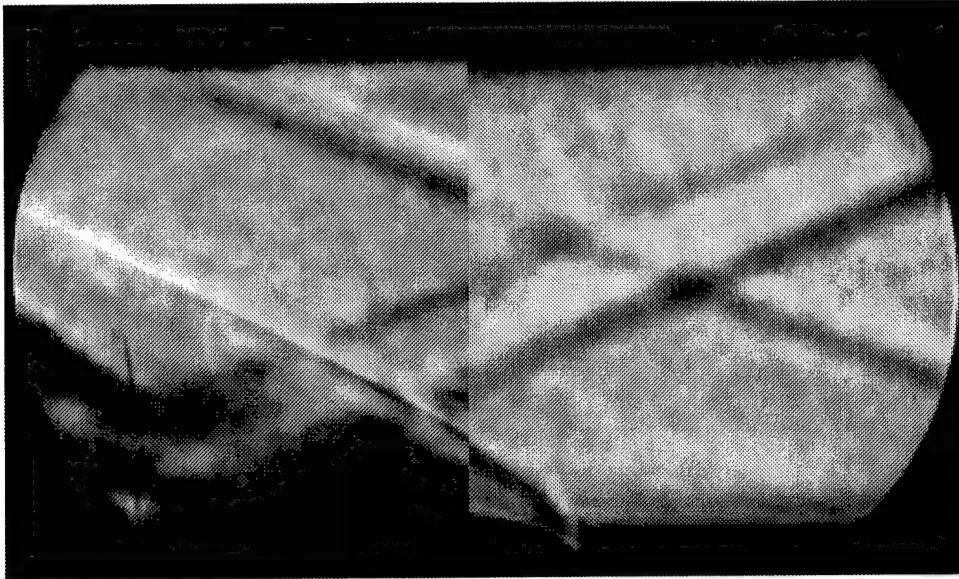


Figure 5.6: Schlieren photograph of argon injection with no ramp

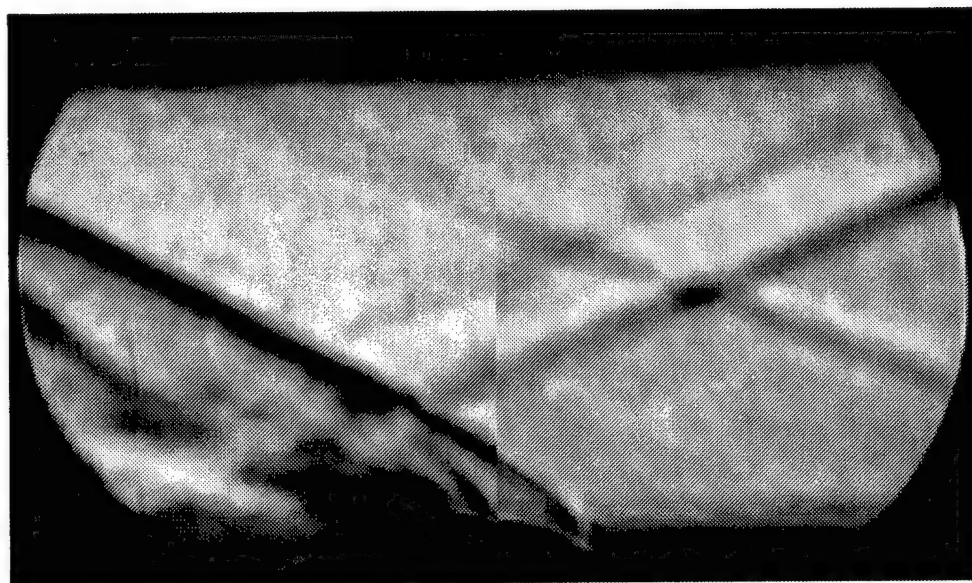


Figure 5.7: Schlieren photograph of argon injection with ramp

5.2.2 Concentration

Figure 5.8 shows the molar concentration data for argon. Again, we see that the no ramp case has a larger area of high concentration argon. Both cases concentrate the argon around the outer edge of the plume. This was not seen with helium and is attributed to the higher molecular weight of argon, where the argon is spun to the outside of the plume by the vortex. The overall plume area for the with-ramp case is 26% larger than without. This is very similar to the 30% seen with air.²² This can be attributed to the similar molecular weight for argon and air. Helium is much lighter than air or argon and therefore the gas mixes into the freestream faster. Air and argon are relatively denser, slower moving gases and are kept within the plume for a longer time.

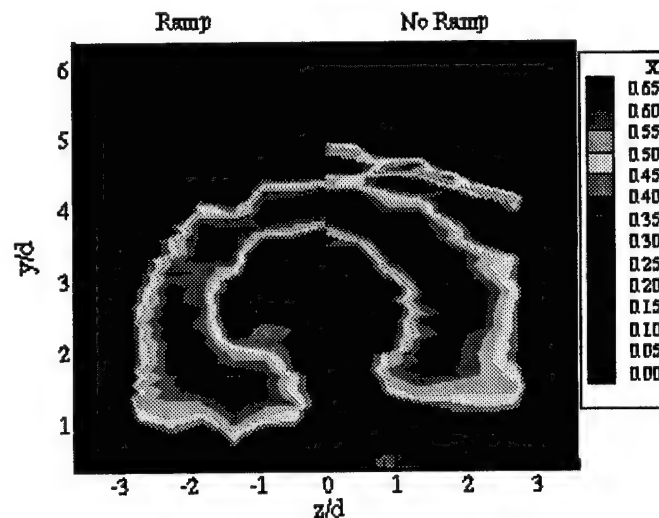


Figure 5.8: Argon concentration contour

5.2.3 Mach

Again as expected, the Mach contour shown in Figure 5.9 shows a larger area of low Mach number within the core of the plume for the ramp case while higher Mach numbers

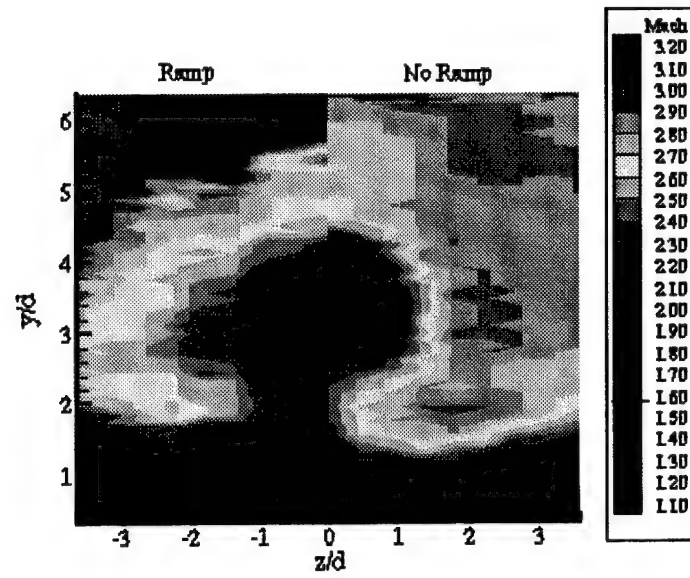


Figure 5.9: Argon Mach contour

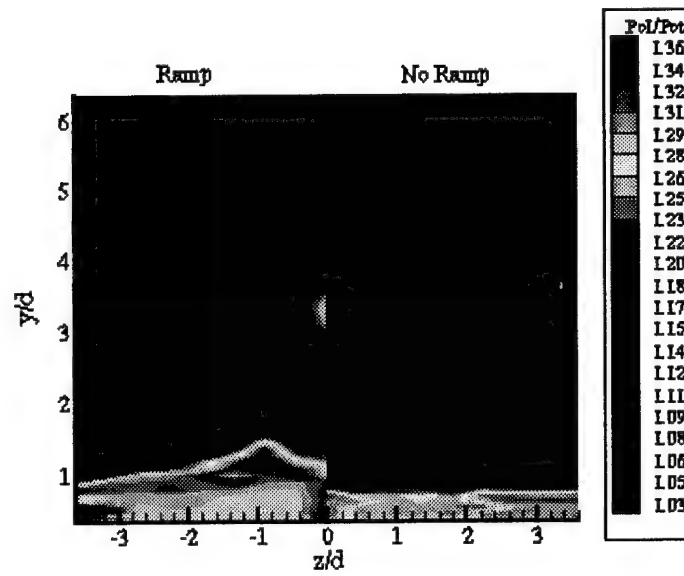


Figure 5.10: Argon total pressure ratio

are seen without the ramp. The plume size was found to be 42% larger with the ramp, giving consistent results with the plume area measured with concentration. This is also about the same size plume found with air injection.²² The effect of molecular weight can be seen in figure 5.9. Air and argon have similar weights and the Mach contours are similar, while the lighter helium has a much larger plume area as indicated in figure 5.4.

5.2.4 Pressure Data

Figure 5.10 shows a comparison of the total pressure ratio for argon injection with and without the PME ramp. The ramp clearly increases the ratio within the plume as was also seen with helium. This data is consistent with prior study results as expected.²²

5.3 Gas Comparison

In both the ramp and no ramp cases, helium provides the greatest mixing. The Mach number determined plume size when compared with air, was three time larger with helium as the injectant. Argon produced a plume about the same size as air. This larger plume size indicates greater mixing and penetration of the plume into the flowfield. Therefore molecular weight does effect the mixing and penetration of the injectant into the freestream.

6. Conclusions and Recommendation

This chapter outlines the primary conclusions drawn from the analysis in Chapter Five. Recommendations for further study are submitted.

6.1 Conclusions

As previously stated, the primary objective of the investigation was to determine the differences molecular weight would cause on mixing and penetration of a gas injecting into a supersonic freestream. The experimental results show a trend: decreasing molecular weight increases mixing and penetration in a simple transverse injection with a PME ramp.

In general, the concentration and Mach plots show agreement with expected results. The PME ramp performed as had been demonstrated in prior studies. The differences in the injectants are clear. The lower molecular weight allows for greater mixing and penetration of the plume into the freestream.

6.2 Recommendation

Results have been established which clearly indicate the trends associated with the effects of molecular weight on mixing and penetration. The next step in conducting the experiment is to continue using helium and to further explore the use of PME ramps. Hydrogen is the most likely candidate for SCRAMjet applications due to the cooling possibilities. Therefore, fully exploring the effects of low molecular weight would be beneficial.

Additional methods can be added to this investigation to provide a more complete view of the flow structures. Laser imagery can be used to enhance the flow visualization to better interpret the flow data. Also, hot wire anemometry can be used to directly measure the

strength of vorticity and turbulent properties. This would allow complete characterization of the flow.

Finally, a continuation of the techniques employed in this investigation is recommended. A study of the trends of molecular weight and PME effects have been tested and evaluations made. Future research can be focused on broadening the basic understanding of the complex flow fields, perhaps in the presence of combustion. Once a suitable base of knowledge exists, refinement of the design choices of fuel and mixing enhancers can lead to optimum configurations.

Appendix A: Uncertainty Analysis

A.1 Position Uncertainty

The measurements conducted in this experiment were made in two dimensions. In the horizontal direction, the positions for measurement were determined using a steel ruler and a point relative to the tunnel floor. The ruler was graduated into 0.7938 cm divisions. A maximum misalignment of $\frac{1}{2}$ of the axial station separation distance would be possible based upon the ruler graduation. This translates into a maximum z axis position uncertainty of ± 0.08 cm.

For each z axis station, a probe sweep of 2.45 cm of the tunnel cross section was made by the traverse system. The vertical position of the probe was tracked by the LVDT system described in section 3.5.2. The position indicated by the LVDT voltage had a recorded variance of $\pm 0.13\%$. This error is deemed insignificant when compared with the horizontal position error.

A.2 Pressure Data Uncertainty

The acquired mean flow pressure data have two associated uncertainties related to gain uncertainty and gain stability across the measurement range. The gain uncertainty was 0.5% and the stability uncertainty was 0.2%. Including digital conversion effects, Huffman found the overall pressure uncertainty was 0.54%. McCann found the Mach number error for similar measurements to be 7%.²²

A.3 Gas Analyzer Uncertainty

The uncertainty of the concentration measurement was previously determined by Fuller to be $\pm 0.2\%$ in mole fraction, and an estimated three percent uncertainty in the calibration curve fit and interpolation routine.²³ This results in a total uncertainty of ± 0.05 in the mole fraction.

Vitae

Captain Troy A. Giese was born 13 November 1970 in Houston, Texas to Charles A. and Deanna Giese. He graduated from Robert E. Lee High School in Midland, Texas in 1989. He graduated from the United States Air Force Academy in Colorado Springs, Colorado and was commissioned into the Air Force in 1993.

Captain Giese's first assignment was to the Delta II Launch Vehicle System Program Office at Los Angeles Air Force Base, California where he served as a propulsion engineer. He also served in the Commander's Action Office for one year. In May of 1996, Captain Giese entered the School of Engineering, Air Force Institute of Technology.

Permanent Address: 5055 Spreen Road
Brenham, TX 77833

Bibliography

1. Curran, E.T., "The Potential and Practicality of High Speed Combined Cycle Engines," Hypersonic Combined Cycle Propulsion, AGARD Conference Proceedings No. 479, 1990, AGARD, Neuilly-Sur-Seine, France, pp. K, pp. 1-9.
2. Heiser, W.H. and D.T. Pratt, Hypersonic Airbreathing Propulsion, American Institute of Aeronautics and Astronautics, Washington, DC, 1994.
3. Anderson, John D., Jr., Hypersonic and High Temperature Gas Dynamics, McGraw Hill, New York, 1989.
4. "Air Force may reprogram FY98 \$ for spaceplane," Military Space, Oct 27 1997, Vol. 14, No. 22, Pasha Publications.
5. Billig, F.S., R.C. Orth, and M. Lasky, "A Unified Analysis of Gaseous Jet Penetration", AIAA Journal, Vol. 9, No. 6, June 1971, pp. 1048-1057.
6. Schetz, J.A. and F.S. Billig, "Penetration of Gaseous Jets Injected into a Supersonic Stream, Journal of Spacecraft and Rockets, Vol. 3, No. 11, November 1966, pp. 1658-1665.
7. Hollo, S.D., J.C. McDaniel and R.J. Harfield, "Quantitative Investigation of Compressible Mixing: Staged Transverse Injection into Mach 2 Flow", AIAA Journal, Vol. 32, No. 3, March 1994, pp. 528-534.
8. Waitz, Ian A., F.E. Marble and E.E. Zukoski, "Investigation of a Contoured Wall Injector for Hypervelocity Mixing Augmentation" AIAA Journal, Vol. 31, No. 6, June 1993, pp. 1014-1021.
9. Schetz, J.A., R.H. Thomas and F.S. Billig, Mixing of Transverse Jets and Wall Jets in Supersonic Flow, Springer-Verlag, Berlin, 1991.
10. Ramakrishnan, R. and D.J. Singh, "Modeling SCRAMjet Combustor Flowfields with a Grid Adaptation Scheme", AIAA Journal, Vol. 32, No. 5, May 1994, pp. 930-935.
11. Grasso, F. and V. Magi, "Simulation of Transverse Gas Injection in Turbulent Supersonic Air Flows", AIAA Journal, Vol. 33, No. 1, January 1995, pp. 56-62.
12. Riggins, D.W. and P.H. Vitt, "Vortex Generation and Mixing in Three-dimensional Supersonic Combustors", Journal of Propulsion and Power, Vol. 11, No. 3, May-Jun 1995, pp. 419-425.
13. Donohue, J.M., J.C. McDaniel, Jr., and Hossein Haj-Hariri, "Experimental and Numerical Study of Swept Ramp Injection into a Supersonic Flowfield", AIAA Journal, Vol. 32, No. 9, September 1994, pp. 1860-1867.

Bibliography

1. Curran, E.T., "The Potential and Practicality of High Speed Combined Cycle Engines," Hypersonic Combined Cycle Propulsion, AGARD Conference Proceedings No. 479, 1990, AGARD, Neuilly-Sur-Seine, France, pp. K, pp. 1-9.
2. Heiser, W.H. and D.T. Pratt, Hypersonic Airbreathing Propulsion, American Institute of Aeronautics and Astronautics, Washington, DC, 1994.
3. Anderson, John D., Jr., Hypersonic and High Temperature Gas Dynamics, McGraw Hill, New York, 1989.
4. "Air Force may reprogram FY98 \$ for spaceplane," Military Space, Oct 27 1997, Vol. 14, No. 22, Pasha Publications.
5. Billig, F.S., R.C. Orth, and M. Lasky, "A Unified Analysis of Gaseous Jet Penetration", AIAA Journal, Vol. 9, No. 6, June 1971, pp. 1048-1057.
6. Schetz, J.A. and F.S. Billig, "Penetration of Gaseous Jets Injected into a Supersonic Stream, Journal of Spacecraft and Rockets, Vol. 3, No. 11, November 1966, pp. 1658-1665.
7. Hollo, S.D., J.C. McDaniel and R.J. Harfield, "Quantitative Investigation of Compressible Mixing: Staged Transverse Injection into Mach 2 Flow", AIAA Journal, Vol. 32, No. 3, March 1994, pp. 528-534.
8. Waitz, Ian A., F.E. Marble and E.E. Zukoski, "Investigation of a Contoured Wall Injector for Hypervelocity Mixing Augmentation" AIAA Journal, Vol. 31, No. 6, June 1993, pp. 1014-1021.
9. Schetz, J.A., R.H. Thomas and F.S. Billig, Mixing of Transverse Jets and Wall Jets in Supersonic Flow, Springer-Verlag, Berlin, 1991.
10. Ramakrishnan, R. and D.J. Singh, "Modeling SCRAMjet Combustor Flowfields with a Grid Adaptation Scheme", AIAA Journal, Vol. 32, No. 5, May 1994, pp. 930-935.
11. Grasso, F. and V. Magi, "Simulation of Transverse Gas Injection in Turbulent Supersonic Air Flows", AIAA Journal, Vol. 33, No. 1, January 1995, pp. 56-62.
12. Riggins, D.W. and P.H. Vitt, "Vortex Generation and Mixing in Three-dimensional Supersonic Combustors", Journal of Propulsion and Power, Vol. 11, No. 3, May-Jun 1995, pp. 419-425.
13. Donohue, J.M., J.C. McDaniel, Jr., and Hossein Haj-Hariri, "Experimental and Numerical Study of Swept Ramp Injection into a Supersonic Flowfield", AIAA Journal, Vol. 32, No. 9, September 1994, pp. 1860-1867.

REPORT DOCUMENTATION PAGE			Form Approved OMB No. 0704-0188	
Public reporting burden for this collection of information is estimated to average 1 hour per response, including the time for reviewing instructions, searching existing data sources, gathering and maintaining the data needed, and completing and reviewing the collection of information. Send comments regarding this burden estimate or any other aspect of this collection of information, including suggestions for reducing this burden, to Washington Headquarters Services, Directorate for Information Operations and Reports, 1215 Jefferson Davis Highway, Suite 1204, Arlington, VA 22202-4302, and to the Office of Management and Budget, Paperwork Reduction Project (0704-0188), Washington, DC 20503.				
1. AGENCY USE ONLY (Leave blank)		2. REPORT DATE December 1997		3. REPORT TYPE AND DATES COVERED Master's Thesis
4. TITLE AND SUBTITLE Experimental Investigation of the Influence of Molecular Weight on Mixing and Penetration in Supersonic Dissimilar Gaseous Injection into a Supersonic Crossflow			5. FUNDING NUMBERS	
6. AUTHOR(S) Troy A. Giese, Capt, USAF				
7. PERFORMING ORGANIZATION NAME(S) AND ADDRESS(ES) AFIT/ENY Air Force Institute of Technology WPAFB OH 45433-6583 Dr. Dana Glawe			8. PERFORMING ORGANIZATION REPORT NUMBER AFIT/GAE/ENY/97D-03	
9. SPONSORING/MONITORING AGENCY NAME(S) AND ADDRESS(ES) Wright Laboratory WL/POPT Bldg. 18, Area B WPAFB OH 45433-7251 Dr Mark Gruber			10. SPONSORING/MONITORING AGENCY REPORT NUMBER	
11. SUPPLEMENTARY NOTES Advise Dr Rodney Bowersox				
12a. DISTRIBUTION AVAILABILITY STATEMENT Approved for public release, distribution unlimited			12b. DISTRIBUTION CODE A	
13. ABSTRACT (Maximum 200 words) In pursuit of a more efficient and effective fuel-air mixing for a SCRAMjet combustor, this study investigated relative near field effects of molecular weight on mixing and penetration of different gaseous injection into a supersonic ($M=2.9$) cross flow. Helium and argon gas were chosen as injectants because of the large differences in molecular weights. Also, mixing enhancement was observed by injecting the traverse gas jet parallel to the compression face of a ramp. Color schlieren photography was used to identify the shock structures and interactions in the flow field. Measurements of mean flow properties were used to establish the jet plume size, penetration, and concentration and to quantify the total pressure loss. Results indicate greater mixing and plume expansion can be achieved with helium compared to argon.				
14. SUBJECT TERMS Propulsion Systems, SCRAMjet, Hypersonic Aircraft Engine, Injection			15. NUMBER OF PAGES 52	
			16. PRICE CODE	
17. SECURITY CLASSIFICATION OF REPORT Unclassified	18. SECURITY CLASSIFICATION OF THIS PAGE Unclassified	19. SECURITY CLASSIFICATION OF ABSTRACT Unclassified	20. LIMITATION OF ABSTRACT UL	